Journal of Materials Chemistry C

ROYAL SOCIETY OF CHEMISTRY

PAPER

View Article Online
View Journal | View Issue

Check for updates

Cite this: J. Mater. Chem. C, 2020, 8, 12829

Bi-functional sulphonate-coupled reduced graphene oxide as an efficient dopant for a conducting polymer with enhanced electrochemical performance†

Lingyin Meng, Frida Dagsgård, Anthony P. F. Turner‡ and Wing Cheung Mak *

The rapidly emerging field of organic bioelectronics has witnessed the wide use of conducting polymers (CPs) to fabricate advanced chemically modified electrodes (CMEs) for biosensors and biomedical devices. The electrochemical performance of the CPs in such devices is closely related to the quality and physiochemical nature of the dopants. A bi-functional graphene oxide derivative with high reduction degree and negatively-charged sulphonate functionality, *i.e.* sulphonate-coupled reduced graphene oxide (S-RGO), was developed and used as an efficient dopant for a CP with enhanced electrochemical performance. The S-RGO was synthesised *via* a facile one-pot hydrothermal reaction using 4-hydrazinobenzosulphonic acid (4-HBS) as reductant and sulphonate precursor simultaneously. The resulting S-RGO possesses high aqueous dispersion stability (more than 6 months), high electrical conductivity (1493.0 S m^{-1}) and sulphonate functionality. Due to these specific properties, S-RGO demonstrated improved electropolymerisation efficiency for poly(3,4-ethylenedioxythiophene) (PEDOT) proving an effective dopant for the preparation of a PEDOT:S-RGO film (5 mC) with faster polymerisation time (37 s) compared to the conventional 2D dopants GO (PEDOT:GO, 129 s) and RGO (PEDOT:RGO, 66 s). The resulting PEDOT:S-RGO appeared as a homogenous film with uniformly distributed S-RGO dopant, low equivalent series resistance and low charge transfer resistance. Moreover, the electrochemical transduction performance of the PEDOT:S-RGO interface was evaluated with 4 different analytes, including ferric/ferrocyanide redox probe, dopamine, nicotinamide adenine dinucleotide and hydrogen peroxide. As a result of the synergistic effect of S-RGO and PEDOT, the PEDOT:S-RGO demonstrated enhanced electrochemical performance with respect to faster electrode kinetics (smaller ΔE_p), ~2 and ~4 times increased current responses, and lower peak potentials compared to PEDOT:GO and PEDOT:RGO. This bi-functional S-RGO dopant combined the advantages of conventional GO and RGO to deliver sulphonate functionality and high conductivity for the preparation of advanced PEDOT interface with improved electrochemical performance, that could potentially be applied for applications in electrochemical sensors, biosensors and bioelectronic devices.

Received 19th May 2020,
Accepted 25th June 2020

DOI: 10.1039/d0tc02402c

rsc.li/materials-c

Open Access Article. Published on 25 giugno 2020. Downloaded on 18/07/2025 22:26:41.
This article is licensed under a Creative Commons Attribution 3.0 Unported Licence.

1. Introduction

Chemically modified electrodes (CMEs) have been widely researched for applications ranging from sensing/biosensing to energy storage, including capacitators and batteries.[1] In recent decade, conducting polymers (CPs) have shown their great potential as an emerging material for CMEs in sensing and biosensing by the virtue of their fascinating electronic and ionic conductivity in a doped state, reversibility, and their unique optical and mechanical properties.[2] CPs, especially for the most commonly studied poly(3,4-ethylenedioxythiophene) (PEDOT), have been extensively employed for electrode modification for the determination of analytes based on their changes in doping/dedoping states, conformation and charge transfer *etc.*[3] For instance, Dong-Sik *et al.*[4] reported a robust PEDOT hydrogel electrode coating layer incorporating cytokine-specific antibodies (Abs) for the detection of inflammatory cytokine, in which the binding of cytokine antigen to the Abs caused a quantifiable change in the electrochemical redox properties of the PEDOT. Meng *et al.*[5] reported a nanofibrous PEDOT for catalytic detection of NADH and dehydrogenase-based biosensors.

Biosensors and Bioelectronics Centre, Division of Sensor and Actuator Systems, Department of Physics, Chemistry and Biology, Linköping University, SE-581 83 Linköping, Sweden. E-mail: wing.cheung.mak@liu.se

† Electronic supplementary information (ESI) available. See DOI: 10.1039/d0tc02402c

‡ Current address: Professor Emeritus, SATM, Cranfield University, Bedfordshire, MK430AL, UK.

Open Access Article. Published on 25 giugno 2020. Downloaded on 18/07/2025 22:26:41.
This article is licensed under a Creative Commons Attribution 3.0 Unported Licence.

However, despite the easy formation of a tenacious film on the substrate *via* electrochemical polymerisation, pure CP-modified electrodes have limited catalytic properties towards a variety of analytes and their surface area is low for effective electrochemical transduction, resulting in unsatisfactory electrochemical performance with low sensitivity, poor selectivity and surface fouling *etc.*[6]

To enhance the performance of the CPs for electrochemical signal transduction, various nanomaterials in different dimensional architectures with unique physical–chemical properties, such as carbon-based nanomaterials, metal/metal oxide nanoparticles, dyes, *etc.*, have been incorporated into the CP matrix as negatively-charged dopants integrated to the positively-charged CP backbone during the polymerisation process.[7] The incorporation of these nanomaterials endow CPs with enhanced or even extended electrochemical properties owing to synergistic effects such as increased active surface area, enhanced charge/electron transfer and improved mechanical stability.[6–8] In the meantime, doping of CPs with other materials also brings in less-control of bulky surface morphology with fragile mechanical property, surface defects and non-uniform distribution, especially for large dopant.[9,10] To realise CP composites with high conductivity, uniform distribution of the nanomaterial within the composite and high polymerisation efficiency, several essential prerequisites for the dopant have to be fulfilled including an appropriate conductivity, aqueous dispersibility and colloidal stability, and the right functional groups.

Among various organic and inorganic dopants, 2D graphene and its derivatives including graphene oxide (GO) and its reduced form (reduced graphene oxide, RGO) are emerging two-dimensional (2D) nanomaterials attracted intensive interest as dopants for CPs owing to their unique physicochemical property, high specific surface area and compatibility.[2,11] GO is one kind of sheet-like graphene consisting of aromatic regions and aliphatic regions including hydroxyl (–OH), carboxyl (–COOH), carbonyl (C═O), and epoxide groups. These oxygen-containing functional groups, especially the carboxyl, endow GO with a highly negatively-charged surface in aqueous solution and thus high dispersibility with long-term stability. Hence, the negatively-charged functional groups on the GO surface, with their excellent water dispersibility, could be effectively incorporated into the CP positively-charged backbone as dopant, resulting an evenly distributed CP:GO hybrid. A variety CP:GO hybrids have been developed, including PEDOT:GO, polypyrrole:GO (PPy:GO), polyaniline:GO (PANi:GO), for electrochemical applications in supercapacitor,[12–14] battery[15,16] and sensing/biosensing.[17,18] However, the well-known electronic insulating property of GO would interrupt the conductivity of the hybrid film and retard the electron transfer kinetics for electrochemical performance.[18] Accordingly, chemical reduction of GO into RGO is usually implemented to restore the graphitic structure with the necessary conductivity and electrochemical catalytic activity, and this is applied as dopant for CPs instead of GO.[19,20] For instance, Wang *et al.*[19] reported that reduced GO doped PEDOT (PEDOT:RGO) through electrochemical reduction of the electrodeposited PEDOT:GO possesses higher surface area and lower electrochemical impedance than untreated PEDOT:GO, and thus a higher electrocatalytic activity towards the sensing of dopamine. Wang *et al.*[21] prepared PPy:RGO for supercapacitors with improved charge/discharge current density and cycle stability *via in situ* galvanostatic polymerisation from the pyrrole monomer and hydrazine reduced RGO suspension. However, RGO has a lower content of oxygen moieties and consequently the deprived negatively-charge surfaces tend to agglomerate due to π–π stacking, which affects the doping efficiency of RGO and results in poor homogeneity of the resulting PEDOT:RGO film.[21] Therefore, a new type of bi-functional graphene-based dopant, which combines the advantages of GO and RGO to deliver high conductivity together with the negatively-charged groups required for high efficiency and homogeneous doping into CPs, is necessary.

Herein, we demonstrated a facile preparation of a novel bi-functional sulphonate-coupled reduced graphene oxide (S-RGO) with high reduction degree and negatively-charged sulphonate terminal functional groups as an efficient dopant for CPs with enhanced electrochemical performance. The S-RGO was synthesised through a facile one-pot hydrothermal reaction between GO and 4-hydrazinobenzosulphonic acid (4-HBS). The 4-HBS served as a bi-functional reductant that simultaneously reduced the GO and coupled the sulphonate into the edge and basal plane of GO, thus forming the S-RGO in a single step as shown in Scheme 1a. The resulting S-RGO combined the advantages of GO and RGO with good aqueous dispersibility, high conductivity and negatively-charged sulphonate terminal functionality, which is favourable for effective doping and electropolymerisation of EDOT to synthesise PEDOT:S-RGO (Scheme 1b). The PEDOT:S-RGO exhibited enhanced electrochemical performance compared to the non-functionalised GO (PEDOT:GO) and RGO (PEDOT:RGO), as demonstrated by various examples including electrochemical detection of the probe/mediator ferric/ferrocyanide ($Fe(CN)_6^{3-/4-}$), the chemical neurotransmitter dopamine (DA), the dehydrogenase co-enzyme nicotinamide adenine dinucleotide (NADH) and hydrogen peroxide (H_2O_2), which is generated from reactions catalysed by oxidase. This facile one-pot hydrothermal synthesised bi-functional S-RGO dopant could overcome the limitations of conventional GO (low conductivity) and RGO (lacking of functionality) dopants and potentially be applied to other CPs such as polypyrrole and polyaniline for the development of advanced CP composites for various organic bioelectronic devices.

2. Experimental section

2.1 Materials

Natural graphite flakes (99.8%, 325 mesh) were purchased from Alfa Aesar (Germany). 4-Hydrazinobenzosulphonic acid hemihydrate ($C_6H_8N_2O_3S{\cdot}1/2H_2O$, 98%) (4-HBS) was purchased from Fisher Scientific (Sweden). Sulphuric acid (H_2SO_4, 97%), potassium persulphate ($K_2S_2O_8$), phosphorus pentoxide (P_2O_5), potassium permanganate ($KMnO_4$), hydrogen chloride (H_2O_2, 30%), hydrochloride acid (HCl), potassium ferricyanide ($K_3[Fe(CN)_6]$),

 This journal is © The Royal Society of Chemistry 2020

Open Access Article. Published on 25 giugno 2020. Downloaded on 18/07/2025 22:26:41.
This article is licensed under a Creative Commons Attribution 3.0 Unported Licence.

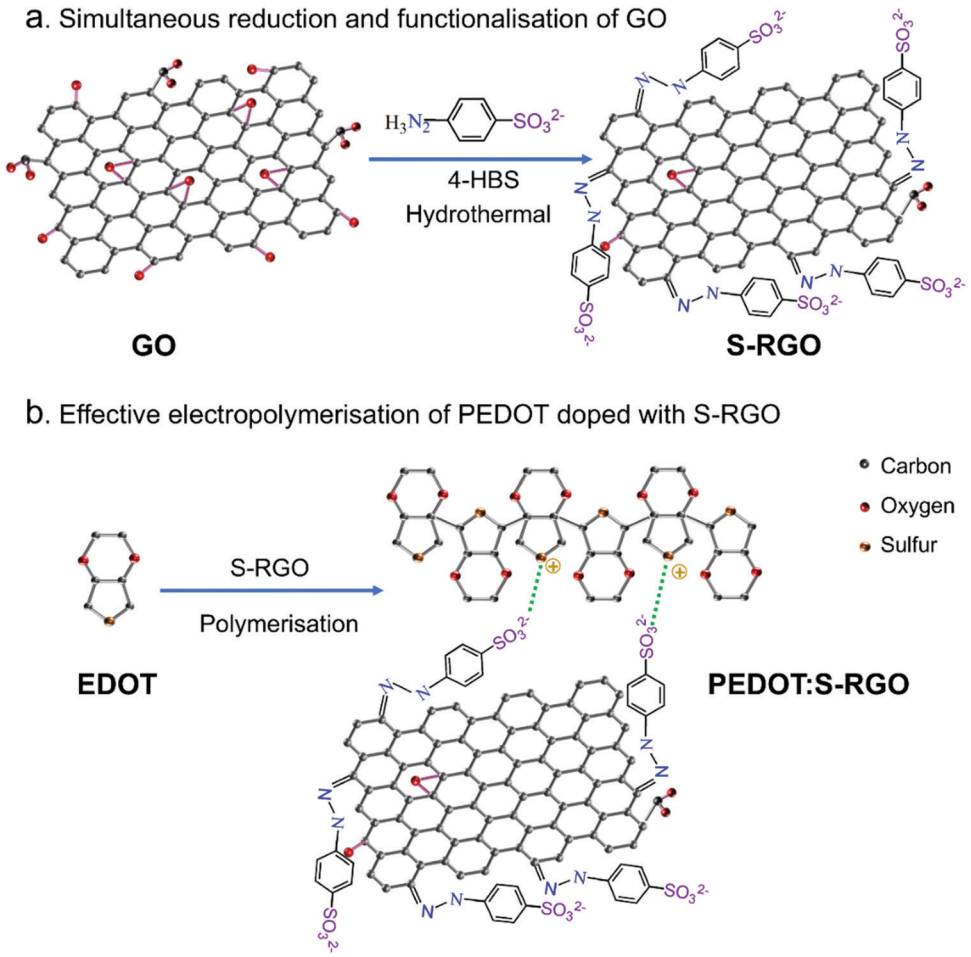

Scheme 1 Schematic illustration of (a) bi-functionalisation of GO to S-RGO *via* one-pot hydrothermal reduction and sulphonate terminal functionality using 4-HBS, (b) effective electropolymerisation of PEDOT using S-RGO as dopant.

potassium ferrocyanide ($K_4[Fe(CN)_6]$), hexaamineruthenium(II/III) chloride ($[Ru(NH_3)_6]Cl_{3/2}$), 3,4-ethylenedioxythiophene (EDOT), dopamine hydrochloride (DA) and nicotinamide adenine dinucleotide reduced form (NADH), were purchased from Sigma-Aldrich (USA). Phosphate buffer solution (PBS, pH 7.4, 0.1 M) was prepared by mixing K_2HPO_4 and NaH_2PO_4 stock solution. All chemicals were of analytical grade and used without any further treatment. Deionised water (DI-water) from a Milli-Q System was used throughout.

2.2 One-pot hydrothermal synthesis of S-RGO

GO was synthesised from natural graphite flakes *via* a modified Hummers' method.[22] S-RGO were realised simultaneously with 4-HBS as reductant and sulphonate processor *via* hydrothermal reaction. In brief, GO (50 mg) was dispersed in 25 mL DI-water by sonicating for 1 h, followed by the addition of 4-HBS (1 g) into the GO suspension under vigorous magnetic stirring for 10 min. Then the mixture was sealed in a 50 mL Teflon-lined autoclave and heated to 140 °C for 6 h. After cooling to room temperature, the product was washed twice with DI-water and ethanol by centrifuging at 8251 × *g* for 15 minutes. The final product was dried in a vacuum oven at 60 °C for 12 h and denoted as S-RGO. As comparison, RGO without sulphonate functionality was synthesised by sodium borohydride according to our previous report.[23,24]

2.3 S-RGO as dopant for PEDOT electropolymerisation

The S-RGO was used as the dopant for PEDOT electropolymerisation in the absence of supporting electrolyte. Prior to electropolymerisation, 10 mM EDOT monomer was dispersed into S-RGO suspension (1 mg mL^{-1}) by sonication for 30 min. The 3 mm glassy carbon electrode (GCE, 0.0707 cm^2) was carefully polished with 0.3 and 0.05 μm aluminum slurries and cleaned with deionised water under sonication. Electropolymerisation was carried out with a fixed potential of 1.2 V and terminated until when the charge reached 5 mC. The electrode was then rinsed in DI-water and denoted as PEDOT:S-RGO. As comparisons, PEDOT:GO and PEDOT:RGO were prepared with the same procedure. Au-coated Si was used as an alternative working electrode for characterisation.

2.4 Characterisation and electrochemical measurements

Scanning electron microscopy (SEM) images were recorded using a LEO 155 Gemini (Zeiss, Germany). The chemical composition was determined by energy-dispersive X-ray spectroscope (EDS,

Open Access Article. Published on 25 giugno 2020. Downloaded on 18/07/2025 22:26:41.
This article is licensed under a Creative Commons Attribution 3.0 Unported Licence.

Oxford Instruments). The zeta potential (surface charge) was recorded using a Zetasizer Nano ZS90 (Malvern Instruments Ltd, UK) in 1 mM of NaCl. Fourier transform infrared (FTIR) spectroscopy was performed using a VERTEX spectrometer (Bruker, USA) equipped with an attenuated total reflection (ATR) measuring cell. UV-vis absorption spectra were measured using a UV-2450 Spectrophotometer (Shimadzu, Japan). X-ray photoelectron spectroscopy (XPS) was acquired with an Axis Ultra DLD instrument (Kratos Analytical, UK) equipped with a monochromatic Al Kα X-ray radiation (hm = 1486.6 eV). Quantification and deconvolution were performed by Casa XPS software (Casa Software Ltd). The sheet resistance of the S-RGO, RGO and GO filtered films were measured using a 4-point probe sheet resistivity meter (Model 280C, Four Dimensions Inc., USA). The electrical conductivity was calculated based on the sheet resistance and thickness. Roughness measurements were performed with a Dektak 6 M surface profilometer (Veeco Inc., USA) with a scanning range of 6000 μm.

All electrochemical measurements were performed with a CompactStat potentiostat (Ivium, Netherlands) at room temperature with a conventional three-electrode system comprising a platinum wire as the counter electrode, a glassy carbon working electrode, and a silver/silver chloride (Ag/AgCl) electrode as the reference. Electrochemical characterisation of S-RGO was performed by drop-casting 5 μL of S-RGO suspension (1 mg mL^{-1}) on a GCE surface (S-RGO/GCE) and drying at room temperature. GO/GCE was prepared by the same procedure for comparison. Evaluation of the electrochemical sensing performance was conducted towards $Fe(CN)_6^{3-/4-}$, DA, NADH and H_2O_2. For comparison, electrochemical measurements using PEDOT:GO and PEDOT:RGO were performed with the same procedure.

3. Results and discussion

3.1 Mechanism of one-pot hydrothermal synthesis of S-RGO

To realise the simultaneous reduction and sulphonate functionalisation of GO, 4-HBS carrying a hydrazine moiety and para-benzosulphonic group was chosen as reductant and functionalisation precursor. As shown in Scheme 1a, the hydrazine moiety of 4-HBS serves as a reductant to reduce the oxygen-containing functional groups on the edge and basal plane of GO under an effective hydrothermal reaction at high temperature (140 °C) and pressure (>1 atm), while the para-benzosulphonic acid groups were simultaneously grafted onto RGO sheets *via* hydrazone bonds to S-RGO. The bi-functional S-RGO with sulphonate groups could serve as prominent counter-ions doped into the positively-charged CP backbone because the strong/mild acidity of sulphonate are able to form ion pairs and shield of the radical cation thus speeding up the polymerisation processes with similar function as polystyrene-sulphonate and tosylate.[25] Moreover, the negatively-charged sulphonate stabilise the colloidal dispersion of S-RGO in aqueous monomer solution, as well as provides good ionic and electrical conductivity, thus facilitating an effective polymerisation of CP with homogenous integration and doping of S-RGO compared to the conventional GO and RGO.

3.2 Characterisation and properties of S-RGO

To achieve good dispersibility is a critical step towards integration of graphene materials as dopant for CPs with high doping efficiency and good homogeneity within the PEDOT-graphene film. As shown in Fig. 1a, both the GO and S-RGO (1 mg mL^{-1}) were well dispersed in water by sonication. After stored for 6 months (Fig. 1b), the GO and S-RGO suspensions remained well-dispersed without observable sediments, indicating a good dispersion stability. The GO suspension was typically brownish-yellow in colour, while the S-RGO suspension forms the typical black-coloured reduced-form of GO, indicating the successful reduction of oxygen-containing groups on GO surface *via* 4-HBS. It is well known that GO with multiple oxygen-containing groups is able to disperse in aqueous solution. Even though the oxygen moieties of the S-RGO were reduced, the inserted sulfonate groups enabled the even dispersion of S-RGO

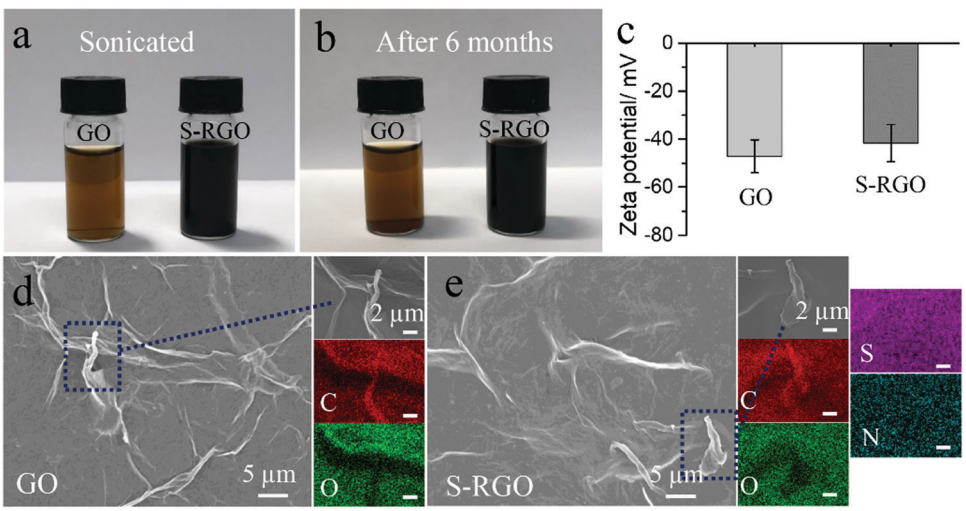

Fig. 1 Digital images of GO and S-RGO aqueous suspensions in 1 mg mL^{-1} just sonicated (a) and after 6 months storage (b); (c) zeta potential of GO and S-RGO aqueous suspensions; SEM images and EDS mapping of GO (d) and S-RGO (e), the scale bar for EDS mapping is 2 μm.

 This journal is © The Royal Society of Chemistry 2020

Open Access Article. Published on 25 giugno 2020. Downloaded on 18/07/2025 22:26:41.
This article is licensed under a Creative Commons Attribution 3.0 Unported Licence.

in aqueous solution. By comparison, RGO without sulphonate functionality by sodium borohydride reduction exhibited poor dispersibility and stability due to the agglomeration of graphene layers *via* π–π stacking (Fig. S1, ESI†). The dispersibility of S-RGO and GO was further qualified by zeta potential analysis in Fig. 1c. The zeta potential of GO was −47.2 ± 6.87 mV, which is attributed to the ionisation of the carboxylic acid groups and is consistent with previously reported values.[26,27] After hydrothermal treatment with 4-HBS, the zeta potential value for S-RGO decreased slightly to −41.7 ± 7.7 mV, which is caused by the coupled sulphonate groups maintaining the negatively-charged property in spite of the intensive reduction of oxygen-containing groups. Nevertheless, the zeta potential value of S-RGO was significantly above ±30 mV, which is considered necessary to deliver a stable colloidal dispersion by interparticle electrostatic repulsion effect.[26,27] On the contrary, the zeta potential value of RGO (−20.9 ± 8.47 mV) is not sufficient to maintain as a stable suspension (Fig. S1, ESI†).

The morphology and chemical composition of S-RGO were characterised by SEM and EDS mapping. The SEM for GO (Fig. 1d) shows a wrinkled and corrugated surface morphology formed by several layers of GO and the corresponding EDS mapping shows a uniform distribution of carbon and oxygen elements on the GO surface. After the hydrothermal reaction with the assistance of 4-HBS, the prepared S-RGO (Fig. 1e) possessed a similar wrinkled surface, suggesting no obvious structural damage caused by the reduction and sulphonate functionalisation under the hydrothermal conditions. EDS mapping of S-RGO revealed sulphur and nitrogen elements originating from the 4-HBS, which was indicative of the successful coupling of sulfonate groups onto the S-RGO.

The reduction degree and sulphonate functionality by 4-HBS during the hydrothermal reaction were investigated using FTIR, UV-vis absorption spectrum and XPS. The FTIR spectrum of GO (Fig. 2a) displayed several characteristic bands for chemical exfoliated GO sheets including O–H stretching vibrations at 3317 cm^{-1}, C═O stretching of carbonyl/carboxyl at 1731 cm^{-1},

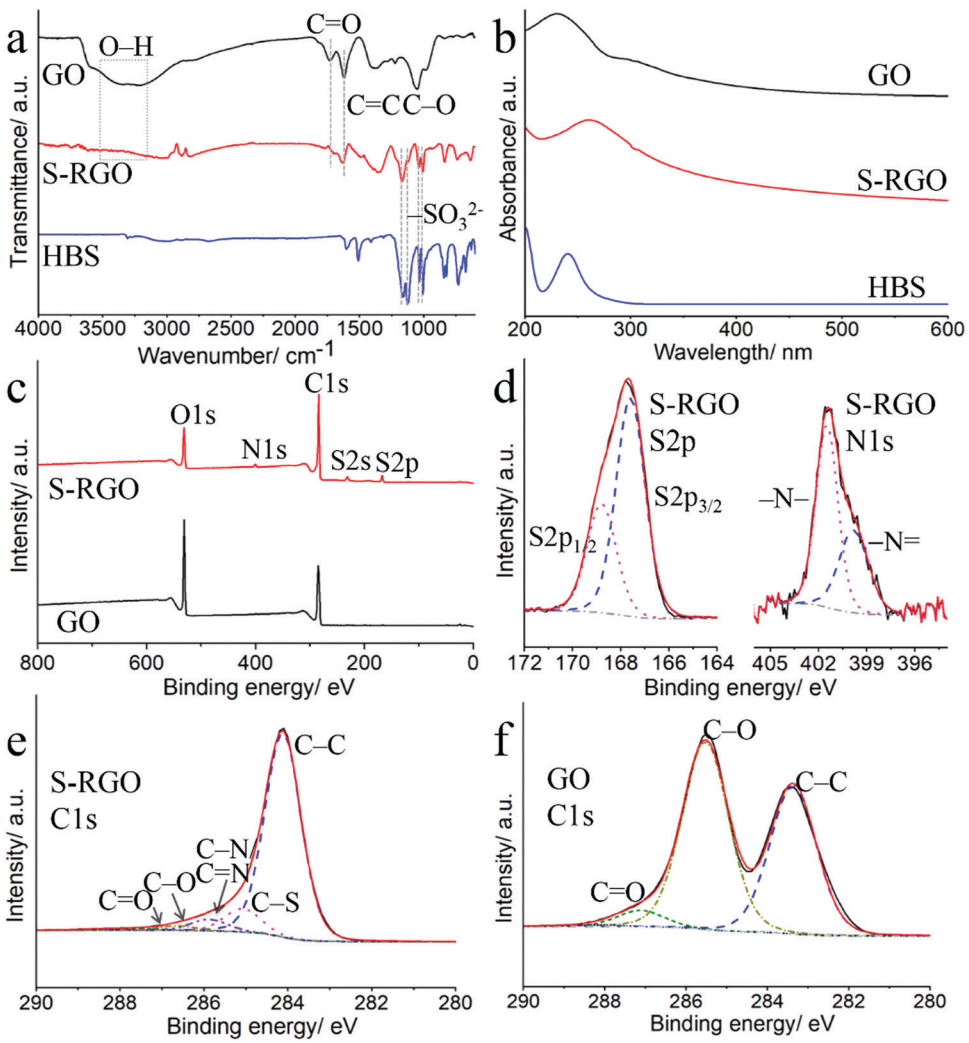

Fig. 2 (a) FTIR spectra and (b) UV-vis spectra of GO, S-RGO and 4-HBS; (c) XPS full survey of GO and S-RGO; (d) XPS S2p and N1s of S-RGO; XPS C1s of S-RGO (e) and GO (f).

Open Access Article. Published on 25 giugno 2020. Downloaded on 18/07/2025 22:26:41.
This article is licensed under a Creative Commons Attribution 3.0 Unported Licence.

C=C skeletal stretching vibrations of the unoxidised graphitic domains and vibration of absorbed water molecules at 1634 cm^{-1}, and C–O stretching vibrations at 1052 cm^{-1}, respectively.[22,23,28] Compared to GO, the intensity of these oxygen-containing bands (O–H, C=O and C–O) at S-RGO decreased dramatically due to the reduction by the hydrazine moiety of 4-HBS.[29] Besides that, the appearance of two sets of bands for S-RGO at 1171/1121 cm^{-1} and 1037/1007 cm^{-1} correspond to the asymmetric and symmetric stretching vibrations of sulfonate ($-SO_3^{2-}$).[30,31] These sets of bands were consistent with the control 4-HBS, indicating the grafting of sulphonate groups on S-RGO. In addition, the UV-vis spectrum of GO (Fig. 2b) contained two distinct bands at 230 nm and 302 nm, which are ascribed to the π–π* transition of the polyaromatic C–C from graphene sheets and n–π* transition of C=O bonds from carbonyl/carboxyl, respectively.[32,33] For S-RGO, the red shifts of the absorption band to 263 nm and the decay of the C=O band provide further evidence of the removal of oxygen-containing groups and restoration of the polyaromatic structure of the graphene sheets.[26]

From the XPS wide survey spectra in Fig. 2c, characteristic sharp bands for C1s and O1s at 284 and 530 eV can be seen for both GO and S-RGO, while new bands for S-RGO at around 167, 231 and 400 eV are assigned to S2p, S2s and N1s, respectively. The detailed deconvolution of the S2p, N1s and C1s with high-resolution scans were shown in Fig. 2d–f. The S2p spectrum of S-RGO (Fig. 2d) consists of spin-split components of $S2p_{3/2}$ (167.6 eV) and $S2p_{1/2}$ (168.8 eV) originating from sulphonate groups, with a spin–orbit separation of 1.2 eV and an intensity ratio of 2 : 1.[34] The deconvoluted N1s (Fig. 2d) components at 399.8 (–N=) and 401.5 eV (–N–) evidenced the formation of hydrazone bonds caused by the hydrazine containing 4-HBS.[35] The hydrazine moiety in 4-HBS serves as reductant for aldehydes/ketones removal on the GO sheets to RGO, and the resulting hydrazone bonds between polyaromatic rings and the para-benzosulphonic acid groups effectively grafted sulphonate groups onto the RGO sheets to produce S-RGO. The C1s spectrum of S-RGO indicates the presence of five deconvoluted carbon bonding states including sp^2-hybridised graphitic C–C (284.1 eV), C–S (285.1 eV) and C–N/C=N (285.7 eV), C–O (286.5 eV) and C=O (287.5 eV).[22,24,36,37] As control, the C1s spectrum of GO consists of only three peaks arising from C–C (283.3 eV), C–O (285.6 eV) and C=O (287.1 eV). The percentage of carbon, oxygen, sulphur and nitrogen elements, and carbon-containing functional groups in S-RGO and GO were listed in Table S1 (ESI†). The dramatic decrease of the O/C atomic ratio from 0.93 for GO to 0.17 for S-RGO, the elimination of oxygen functionalities (*i.e.* C–O, C=O), together with the appearance of S and N attest to simultaneous reduction and sulphonate group functionalisation. Besides, the O/C atomic ratio for S-RGO is also smaller than that of RGO (0.26) driven from sodium borohydride, indicating the higher reduction degree of S-RGO by 4-HBS *via* the one-pot hydrothermal synthesis approach (Table S1 and Fig. S2, ESI†).

3.3 Electrochemical properties of the S-RGO

The electrochemical behaviour of the S-RGO was investigated using two different charged redox probes (*i.e.* negatively-charged $Fe(CN)_6^{3-/4-}$ and positively-charged $[Ru(NH_3)_6]^{2+/3+}$). As shown in Fig. 3, the S-RGO modified electrode show quasi-reversible peaks with a significantly increased redox peak current densities (I_p) and different peak-to-peak separations (ΔE_p) in these two redox probes compared to GO. The I_p and ΔE_p for S-RGO and GO are summarised in Table S2 (ESI†). With the positively-charged $[Ru(NH_3)_6]^{2+/3+}$ probe, the CVs obtained from the GO-modified electrode exhibited an anodic I_p of 4.62 μA and a ΔE_p of 130 mV. For the S-RGO-modified electrode, the anodic I_p showed a dramatic increase by ~19 times up to 87.50 μA and the ΔE_p decreased to 95 mV, indicating facilitated electron and mass transfer at the S-RGO interface. The redox peak currents increased incrementally with cycling for both of the S-RGO and GO (Fig. S3, ESI†), which is ascribed to the electrostatic attraction effect from the negatively-charged sulphonate groups on S-RGO and the carboxylate groups on GO, respectively. When the measurement was performed with the negatively-charged probe $Fe(CN)_6^{3-/4-}$, the anodic I_p and ΔE_p for GO modified electrode were 1.97 μA and 180 mV. The S-RGO electrode showed a ~12 times higher anodic I_p (23.4 μA), while the ΔE_p increased to 215 mV. The ΔE_p of S-RGO modified electrode in negatively-charged $Fe(CN)_6^{3-/4-}$ was the inverse of that of in positively-charged $[Ru(NH_3)_6]^{2+/3+}$. The observed electrochemical behaviors could be attributed to successful integration of the negatively-charged sulphonate groups on the S-RGO, which could attract the opposite charged $[Ru(NH_3)_6]^{2+/3+}$ and repel the similarly charged $Fe(CN)_6^{3-/4-}$.

The electrical conductivity of S-RGO was obtained from the sheet resistance and thickness of a free-standing S-RGO film (Fig. S4, ESI†) prepared by vacuum filtration. As shown in Table 1, the electrical conductivity of S-RGO was calculated to be 1493.0 S m^{-1}, while it was not measurable for GO owing to the electrical insulation. As comparison, the electrical conductivity of RGO derived from sodium borohydride was 158.1 S m^{-1}, which is of the same magnitude with the literature reported value.[38–40] The electrical conductivity of S-RGO is ~10 times higher than that of conventional RGO, which is resulted from the higher reduction degree of S-RGO supported by the XPS result.

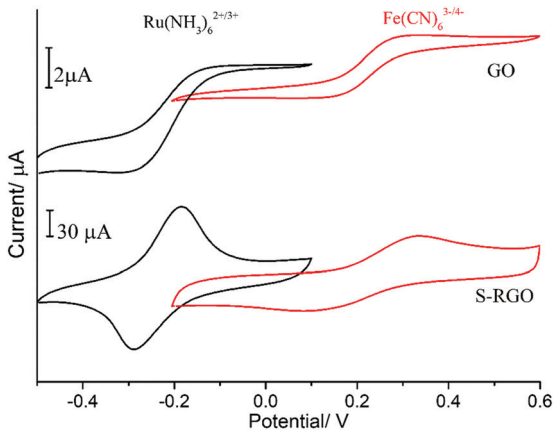

Fig. 3 CVs of GO and S-RGO modified electrodes in 0.1 M KCl containing 5 mM $Fe(CN)_6^{3-/4-}$ or 2 mM $[Ru(NH_3)_6]^{2+/3+}$, scan rate of 50 mV s^{-1}.

This journal is © The Royal Society of Chemistry 2020

Open Access Article. Published on 25 giugno 2020. Downloaded on 18/07/2025 22:26:41.
This article is licensed under a Creative Commons Attribution 3.0 Unported Licence.

Table 1 Electrical conductivity of S-RGO, RGO and GO, and equivalent series resistance (ESR) of PEDOT:S-RGO, PEDOT:RGO and PEDOT:GO modified electrodes

Samples	Conductivity/S m^{-1}	Electrode	ESR/Ω
S-RGO	1493.0	PEDOT:S-RGO	310.9
RGO	158.1	PEDOT:RGO	343.0
GO	—	PEDOT:GO	368.2

3.4 Efficient electropolymerisation of PEDOT doped with S-RGO (PEDOT:S-RGO)

The S-RGO, with its excellent electrochemical properties, high conductivity and sulphonate functionality, was employed as an effective dopant for PEDOT electropolymerisation (Scheme 1b) and compared with GO and RGO. Fig. 4a shows the current–time curve and charge–time curve (inset) recorded during potentiostatic polymerisation at 1.2 V in a mixture of EDOT monomer (10 mM) and GO, RGO and S-RGO (1 mg mL^{-1}) without additional supporting electrolyte until a fixed charge of 5 mC was reached. It can be seen that the polymerisation of PEDOT with the S-RGO suspension (37 s) was significantly faster than that of GO (129 s) and RGO (66 s), revealing that the S-RGO is considerably more efficient for doping into PEDOT to form PEDOT:S-RGO. In addition, the initial spike of current corresponding to the charging of the double layer at S-RGO was 243 μA, which is much larger than those of GO (73 μA) and RGO (39 μA). Moreover, the interfacial capacitance[41] of the resulted PEDOT:S-RGO (Fig. S5, ESI†) was estimated to be 14.4 mF cm^{-2}, which is 2.8 and 7.8 times higher than that of PEDOT:RGO (5.1 mF cm^{-2}) and PEDOT:GO (1.8 mF cm^{-2}), respectively. The increased polymerisation efficiency and higher charging current for PEDOT:S-RGO are most likely attributed to: (1) the increased degree of reduction leading to higher conductivity of S-RGO; (2) sulphonate functionality of S-RGO not only serves as an excellent negatively-charged counter-ion to compensate the charge of PEDOT backbone, but provides the suspension with good ionic conductivity.

Electrochemical impedance spectroscopy (EIS) was performed to evaluate the electrochemical properties for PEDOT:S-RGO, PEDOT:RGO and PEDOT:GO electrodes. Fig. 4c shows the Nyquist plots for all electrodes measured in the frequency range of 100 kHz to 0.1 Hz composed of a semi-circle in the high frequency region and straight line in the low frequency region, which were fitted with the corresponding equivalent electrical circuits (Fig. S6, ESI†). The intercept of the real axis (Z') at the high frequency region of the Nyquist plot is corresponding to the equivalent series resistance (ESR) from the internal resistance of the electrode material and ohmic resistance of the electrolyte.[42–44] Given that the electrical conductivity of electropolymerised PEDOT:graphene film on a conductive substrate cannot be accurately measured using the 4-point probe technique, ESR was employed to compare the electrical characteristic of various PEDOT:graphene composites.

As shown in Table 1, the ESR values for PEDOT:S-RGO, PEDOT:RGO and PEDOT:GO are 310.9, 343.0 and 368.2 Ω, respectively. It is important to note that during the preparation of PEDOT:graphene composites, the main role of S-RGO, RGO and GO are served as counter-ion dopants to support the electropolymerisation of PEDOT backbone, thus PEDOT dominates the conductivity of the PEDOT:graphene composites. Nevertheless, the ESR valve for the PEDOT:S-RGO is smaller than that of PEDOT:RGO and PEDOT:GO, which manifests the improved electrical conductivity originating from the higher conductivity of S-RGO dopant (Table 1, first two columns) and the sulfonate functionality leading to higher PEDOT electropolymerisation efficiency compared to RGO and GO (Fig. 4a).

On the other hand, the semi-circular behavior in the high/mid-frequency region is related to the charge transfer resistance (R_{ct}) at the electrode/electrolyte interface.[42] The bare electrode possesses a large semicircle with a R_{ct} value of 1898.8 Ω. After the electropolymerisation of PEDOT:graphene, the semi-circle decreased dramatically for all the modified electrodes, suggesting an enhanced charge transfer process, and the R_{ct} value for the PEDOT:S-RGO (290.3 Ω) is smaller that of the PEDOT:RGO (317.0 Ω) and PEDOT:GO (432.6 Ω). The improved impedance property of PEDOT:S-RGO than that of PEDOT:RGO and PEDOT:GO could be attributed to the higher conductivity of S-RGO and its improved electropolymerisation efficiency.

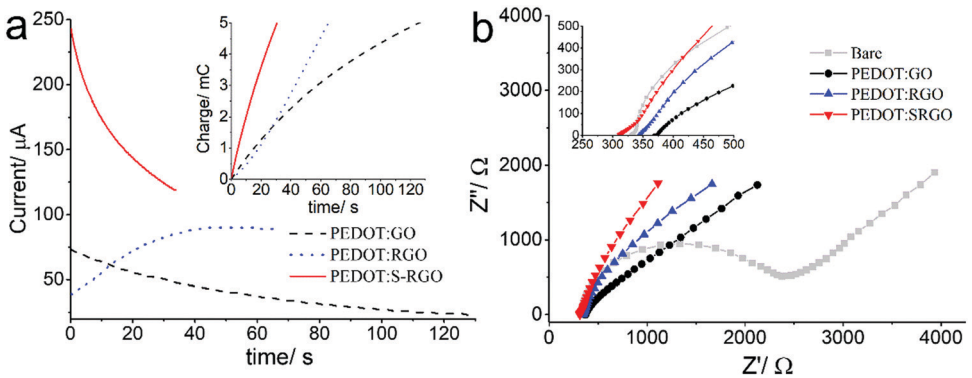

Fig. 4 (a) Potentiostatic–polymerisation curve of PEDOT:GO, PEDOT:RGO and PEDOT:S-RGO, inset is the charge curve; (b) Nyquist plots of bare, PEDOT:GO, PEDOT:RGO and PEDOT:S-RGO modified electrode in 5 mM $Fe(CN)_6^{3-/4-}$ in 0.1 M KCl, inset is the magnified plots in high frequency range.

Open Access Article. Published on 25 giugno 2020. Downloaded on 18/07/2025 22:26:41.
This article is licensed under a Creative Commons Attribution 3.0 Unported Licence.

3.5 Characterisation of the PEDOT:S-RGO

The morphology and surface composition profiles of the PEDOT:S-RGO, PEDOT:GO and PEDOT:RGO were elucidated using SEM, EDS mapping and XPS (Fig. 5). The SEM image of PEDOT:S-RGO (Fig. 5a) shows a homogenously-dispersed film with a wrinkled structure. The C, S and N mappings indicate the homogeneous distribution of the PEDOT and S-RGO components in the film, in which C and S originate from both PEDOT and S-RGO, while N is attributed to the hydrazone bonds in S-RGO. Similar to PEDOT:S-RGO, the PEDOT:GO also displayed a compact and crumpled film with homogenously-dispersed C and S elements (Fig. 5b). In contrast, the PEDOT:RGO had a non-uniformly distributed globular morphology of separated PEDOT particles and RGO flakes. The roughness R_a values (arithmetical mean deviation) from the surface profile (Fig. S7, ESI†) were 0.232, 1.50 and 0.382 μm for PEDOT:GO, PEDOT:RGO and PEDOT:S-RGO, respectively. Owing to the sulphonate moieties on S-RGO and rich oxygen moieties on GO, the S-RGO and GO dopants are well dispersed and evenly integrated into the PEDOT matrix during the electropolymerisation process resulting in the fairly uniform PEDOT composite films. However, the intensive reduction of oxygen in RGO caused the

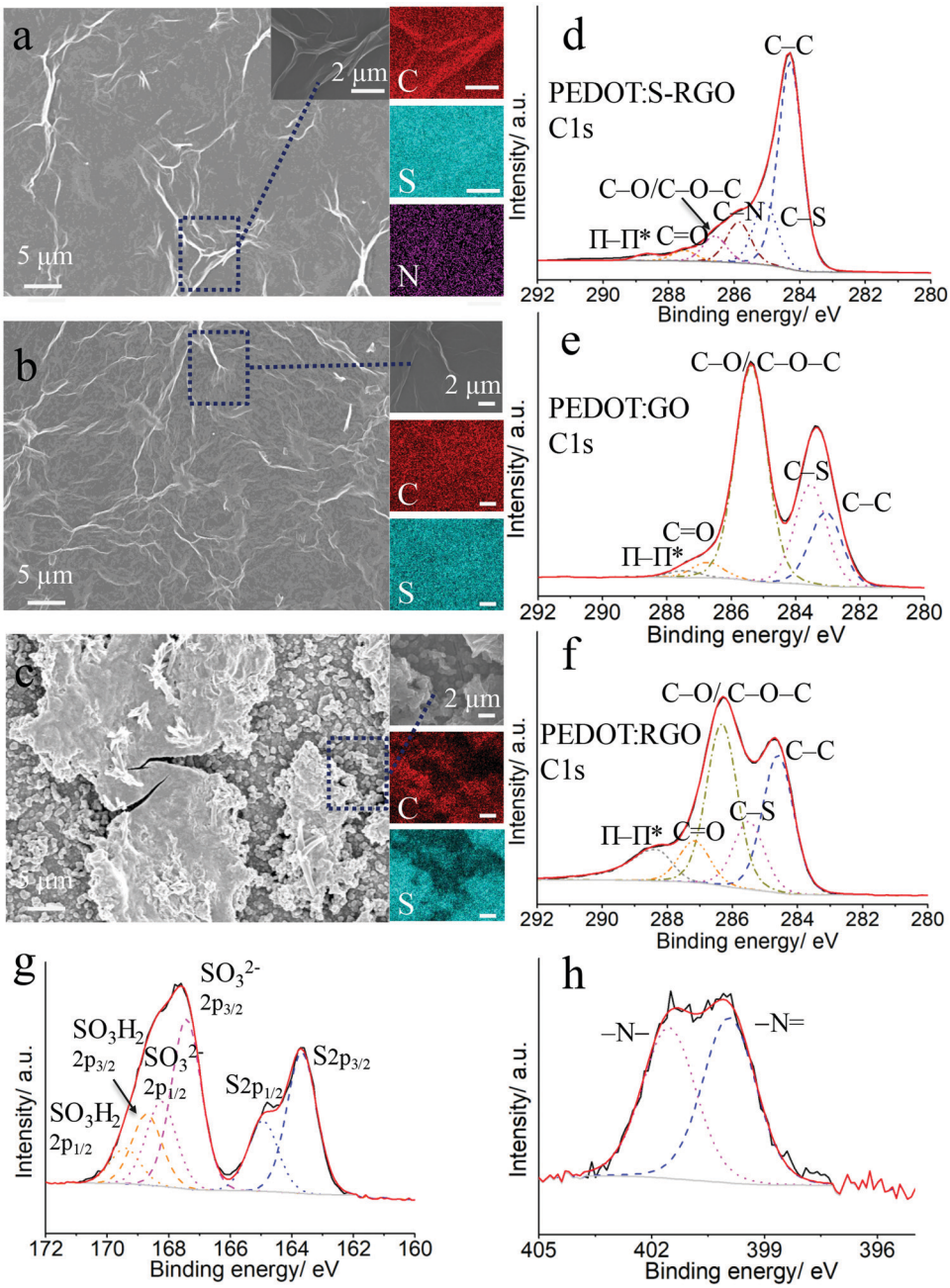

Fig. 5 SEM images and EDS mapping of PEDOT:S-RGO (a), PEDOT:GO (b) and PEDOT:RGO (c), the scale bar for EDS mapping is 2 μm; XPS C1s spectra of PEDOT:S-RGO (d), PEDOT:GO (e) and PEDOT:RGO (f); S2p spectrum (g) and N1s spectrum (h) of PEDOT:S-RGO.

 This journal is © The Royal Society of Chemistry 2020

Open Access Article. Published on 25 giugno 2020. Downloaded on 18/07/2025 22:26:41.
This article is licensed under a Creative Commons Attribution 3.0 Unported Licence.

aggregates in RGO suspension, which is a common problem for RGO, and the resulted PEDOT:RGO showed an irregular distribution of PEDOT and RGO components.

The XPS full survey (Fig. S8a, ESI†) of PEDOT:S-RGO, PEDOT:GO and PEDOT:RGO showed the C1s (285 eV), O1s (532 eV) and S2p (168 eV) elements to be prevalent in PEDOT and GO derivatives, while the N1s at 400 eV for PEDOT:S-RGO arises from S-RGO. The high resolution C1s spectrum for PEDOT:S-RGO (Fig. 5e) was fitted with six components including C–C (284.3 eV), C–S (285.0 eV), C–N (285.8 eV), C–O/C–O–C (286.6 eV), C═O (287.5 eV), O–C═O and π–π* shake-up (288.7 eV). The C–S peak arises from both of the PEDOT and S-RGO, while the appearance of C–N is indicative of the doping of S-RGO into PEDOT backbone. In comparison, the deconvolution of C1s spectrum for PEDOT:GO (Fig. 5e) and PEDOT:RGO (Fig. 5f) yielded similar peaks except the absence of C–N.

In addition, the core level spectra of S2p for PEDOT:S-RGO (Fig. 5g) demonstrates the two main peaks originating from PEDOT (164 eV) and S-RGO (168 eV), respectively. The deconvolution of the main peak at low binding energy corresponds to sulphur from PEDOT as the $S2p_{3/2}$ (163.7 eV) and $S2p_{1/2}$ (164.9 eV) spin–orbit doublet with a characteristically fixed intensity ratio of 2 : 1 and energy splitting of 1.2 eV.[45] The main peak at high binding energy is due to the sulphonate groups in S-RGO, which can be deconvoluted and assigned to doping groups $-SO_3^{2-}$ (spin–orbit doublet at 167.4 eV for $-SO_3^{2-}$ $2p_{3/2}$ and 168.2 eV for $-SO_3^{2-}$ $2p_{1/2}$) and protonated $-SO_3H_2$ (spin–orbit doublet at 168.7 eV for $-SO_3H_2$ $2p_{3/2}$ and 169.4 eV for $-SO_3H_2$ $2p_{1/2}$).[46] Only one set of S2p peak originating from PEDOT moiety can be observed at PEDOT:GO and PEDOT:RGO (Fig. S8b and c, ESI†). In Fig. 5h, the deconvoluted N1s core level spectrum of PEDOT:S-RGO shows two distinct peaks at 399.9 eV and 401.5 eV due to –N═ and –N–, which is consistent with the N1s spectra for S-RGO. As comparison, no obvious N1s peaks were observed at PEDOT:GO and PEDOT:RGO (Fig. S8d and e, ESI†).

3.6 Enhanced electrochemical sensing performance of PEDOT:S-RGO

To evaluate the potential application of PEDOT:S-RGO as an electrochemical interface for sensing and biosensing, we examined CVs with 4 different analytes, including the $Fe(CN)_6^{3-/4-}$ redox probe/mediator, chemical neurotransmitter DA, dehydrogenase co-enzyme NADH and H_2O_2, which is generated by oxidase catalysed reactions. As shown in Fig. 6, PEDOT:S-RGO demonstrated improved electrochemical sensing performance for all of the 4 analytes compared to that of PEDOT:RGO and PEDOT:GO, as indicated by decreased peak-to-peak separations, increased anodic currents, and negatively-shifted oxidation potentials and onset potentials. The key electrochemical parameters for these 4 analytes are summarised in Table 2. For DA, the PEDOT:S-RGO showed improved electrocatalysis with an $I_{p,oxi}$ value of 41.4 μA and ΔE_p of 70 mV, which is 2.0 and 4.4-fold higher than that of PEDOT:RGO (20.4 μA) and PEDOT:GO (9.4 μA). As an important redox mediator/probe for electrochemical catalytic/affinity biosensing, $Fe(CN)_6^{3-/4-}$ underwent faster electron and mass transfer at PEDOT:S-RGO surface with the highest $I_{p,oxi}$ value

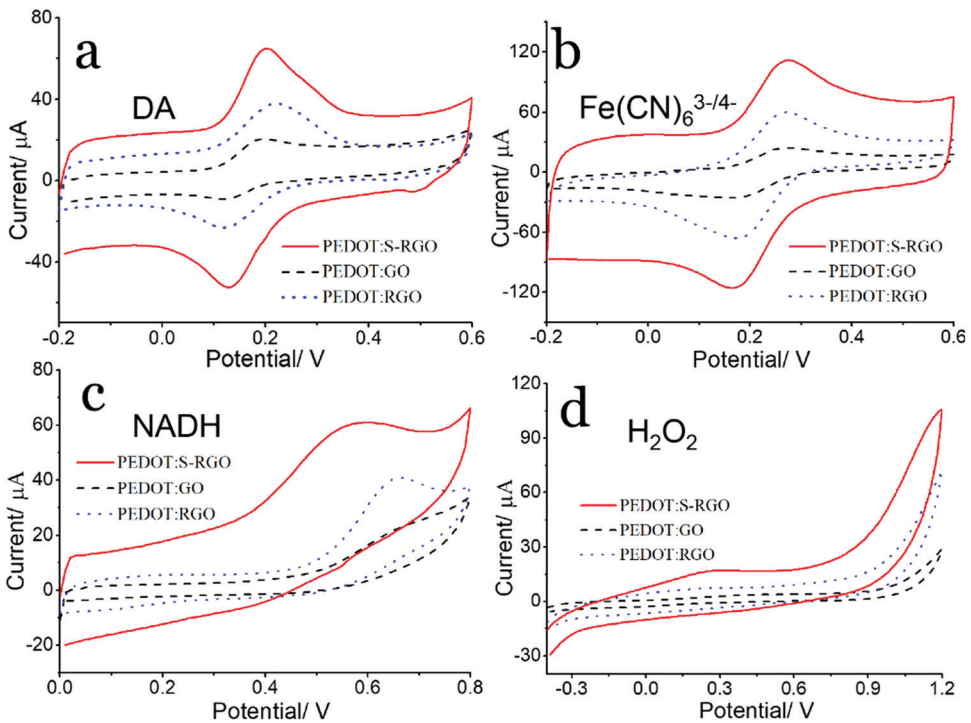

Fig. 6 CVs of (a) 0.5 mM DA in 0.1 M PBS, (b) 5 mM $Fe(CN)_6^{3-/4-}$ in 0.1 M KCl, (c) 5 mM NADH in 0.1 M PBS, (d) 7.8 mM H_2O_2 in 0.1 M PBS at PEDOT:S-RGO, PEDOT:GO and PEDOT:RGO electrodes, scan rate of 50 mV s^{-1}.

Table 2 Summary of electrochemical performance of PEDOT:S-RGO in comparison of PEDOT:RGO and PEDOT:GO for DA, $Fe(CN)_6^{3-/4-}$, NADH and H_2O_2

	DA		$Fe(CN)_6^{3-/4-}$		NADH		H_2O_2	
Electrode	ΔE_p/mV	$I_{p,oxi}$/μA	ΔE_p/mV	$I_{p,oxi}$/μA	$E_{p,oxi}$/V	$I_{p,oxi}$/μA	E_{onset}[a]/V	I_{oxi}[b]/μA
PEDOT:S-RGO	70	41.4	100	74.5	0.590	47.0	0.70	36.4
PEDOT:RGO	95	20.4	110	37.7	0.660	29.1	0.82	17.0
PEDOT:GO	70	9.4	115	17.3	0.690	14.8	0.95	—

Note: [a] E_{onset}: onset potential. [b] I_{oxi}: oxidation current collected at 0.9 V.

Open Access Article. Published on 25 giugno 2020. Downloaded on 18/07/2025 22:26:41.
This article is licensed under a Creative Commons Attribution 3.0 Unported Licence.

of 74.5 μA and lowest ΔE_p of 100 mV in comparison with PEDOT:RGO (37.7 μA, 110 mV) and PEDOT:GO (17.3 μA, 115 mV).

NADH is one of the most important coenzymes in the human body and its measurement can be coupled with NAD-dependent dehydrogenases for the detection of a wide range of metabolites.[31] The $I_{p,oxi}$ value for NADH increased from 14.8 μA at PEDOT:GO to 29.1 μA at PEDOT:RGO and finally up to 47.0 μA at PEDOT:S-RGO, while the oxidation peak potential showed a decreased trend of 0.69, 0.66 and 0.59 V for PEDOT:GO, PEDOT:RGO and PEDOT:S-GO, respectively. The oxidative metabolism product H_2O_2 is another important chemical analytes for oxidase-based biosensing. The E_{onset} for PEDOT:S-RGO electrode was around 0.70 V, which is 120 mV and 250 mV negatively-shifted from 0.82 V and 0.95 V obtained for PEDOT:RGO and PEDOT:GO, respectively. In addition, the oxidation current (measured at 0.9 V) for the PEDOT:S-RGO electrode (36.4 μA) was 2.1 times higher than that for PEDOT:RGO (17.0 μA), while E_{onset} was too high for PEDOT:GO and the oxidation current was not detectable at 0.9 V.

Cumulatively, these results clearly demonstrate that PEDOT:S-RGO offers improved electrochemical performance than conventional PEDOT:GO and PEDOT:RGO by delivering faster electron transfer (smaller ΔE_p), increased current response and lower peak potential for signal transduction. It is noted that the surface morphology of polymer composite might influence the electrochemical performance,[47,48] such that an increased surface roughness provides a relatively higher surface area leading to improve electrochemical performance. From our results, PEDOT:GO and PEDOT:S-RGO displayed similar morphology and roughness proved by SEM and surface profile, the improvement in the electrochemical performance from PEDOT:GO to PEDOT:S-RGO can be ascribed to higher conductivity of S-RGO compared with GO as dopants. In contrast, PEDOT:RGO possesses a rougher surface with relatively higher surface area compared with PEDOT:S-RGO. However, the overall electrochemical performance of the PEDOT:S-RGO remains significantly better than the PEDOT-RGO, demonstrating that the S-RGO bearing sulfonate functionality and high conductivity is an effective dopant for the preparation of PEDOT composites. Moreover, the cyclic stability of the PEDOT:S-RGO, PEDOT:GO and PEDOT:RGO were evaluated by CVs in $Fe(CN)_6^{3-/4-}$ redox probe. All the three electrode retained more than 90% of the peak current after 100 cycles, in which PEDOT:S-RGO demonstrated the best cyclic stability with 98.9% retention after 100 cycles. The improvement in electrochemical performance makes PEDOT:S-RGO attractive for the development of a wide range of sensors/biosensors and bioelectronic devices.

4. Conclusion

We have demonstrated a bi-functional sulphonate functionalised, reduced graphene oxide (S-RGO) prepared by a facile one-pot hydrothermal synthesis with the assistance of 4-HBS as a reductant and functionalisation precursor. Using hydrothermal condition, GO was successfully functionalised with both high reduction degree by the hydrazine moiety of 4-HBS and coupled with sulphonate groups *via* hydrazone bonds to S-RGO. The high conductivity, good aqueous dispersibility and sulphonate functionality of S-RGO made it an ideal dopant for PEDOT electropolymerisation, resulting in improved polymerisation efficiency and electrochemical performance compared to GO and RGO. As a result of the synergistic effect of S-RGO and PEDOT, the resulting PEDOT:S-RGO displayed not only low equivalent series resistance and charge transfer resistance, but enhanced electrochemical performance for $Fe(CN)_6^{3-/4-}$, DA, NADH and H_2O_2 transduction with respect to faster electron transfer (smaller ΔE_p), increased current response and low peak potential. Hence, PEDOT:S-RGO composites provide a superior method for the creation of CMEs with a wide range of potential applications in sensors, biosensors, biofuel cells, bioelectrocatalysis and other bioelectronic devices.

Conflicts of interest

There are no conflicts to declare.

Acknowledgements

The authors would like to acknowledge the Swedish Research Council (VR-2015-04434) and the China Scholarship Council (File no. 201606910036) for generous financial support to carry out this research. The authors would like to thank Dr Grzegorz Greczynski from Thin Film Physics, Linköping University for the conduct of XPS measurements.

References

1 A. J. Bard, *J. Chem. Educ.*, 1983, **60**, 302.
2 M. H. Naveen, N. G. Gurudatt and Y.-B. Shim, *Appl. Mater. Today*, 2017, **9**, 419–433.

 This journal is © The Royal Society of Chemistry 2020

Open Access Article. Published on 25 giugno 2020. Downloaded on 18/07/2025 22:26:41.
This article is licensed under a Creative Commons Attribution 3.0 Unported Licence.

3 H. Yoon and J. Jang, *Adv. Funct. Mater.*, 2009, **19**, 1567–1576.
4 D. S. Shin, Z. Matharu, J. You, C. Siltanen, T. Vu, V. K. Raghunathan, G. Stybayeva, A. E. Hill and A. Revzin, *Adv. Healthcare Mater.*, 2016, **5**, 659–664.
5 L. Meng, A. P. F. Turner and W. C. Mak, *Biosens. Bioelectron.*, 2020, **159**, 112181.
6 S. Shrivastava, N. Jadon and R. Jain, *TrAC, Trends Anal. Chem.*, 2016, **82**, 55–67.
7 L. Meng, A. P. Turner and W. C. Mak, *Biotechnol. Adv.*, 2020, **39**, 107398.
8 G. Wang, A. Morrin, M. Li, N. Liu and X. Luo, *J. Mater. Chem. B*, 2018, **6**, 4173–4190.
9 T. Goda, M. Toya, A. Matsumoto and Y. Miyahara, *ACS Appl. Mater. Interfaces*, 2015, **7**, 27440–27448.
10 W. Hai, T. Goda, H. Takeuchi, S. Yamaoka, Y. Horiguchi, A. Matsumoto and Y. Miyahara, *ACS Appl. Mater. Interfaces*, 2017, **9**, 14162–14170.
11 W. Lei, W. Si, Y. Xu, Z. Gu and Q. Hao, *Microchim. Acta*, 2014, **181**, 707–722.
12 E. Mitchell, J. Candler, F. De Souza, R. K. Gupta, B. K. Gupta and L. F. Dong, *Synth. Met.*, 2015, **199**, 214–218.
13 N. H. N. Azman, H. N. Lim and Y. Sulaiman, *Electrochim. Acta*, 2016, **188**, 785–792.
14 J. Cao, Y. Wang, J. Chen, X. Li, F. C. Walsh, J.-H. Ouyang, D. Jia and Y. Zhou, *J. Mater. Chem. A*, 2015, **3**, 14445–14457.
15 H. Yang, Y. Qiu and X. Guo, *Electrochim. Acta*, 2016, **215**, 346–356.
16 X. Wang, Z. Zhang, X. Yan, Y. Qu, Y. Lai and J. Li, *Electrochim. Acta*, 2015, **155**, 54–60.
17 W. Si, W. Lei, Z. Han, Y. Zhang, Q. Hao and M. Xia, *Sens. Actuators, B*, 2014, **193**, 823–829.
18 I. M. Taylor, E. M. Robbins, K. A. Catt, P. A. Cody, C. L. Happe and X. T. Cui, *Biosens. Bioelectron.*, 2017, **89**, 400–410.
19 W. Wang, G. Xu, X. T. Cui, G. Sheng and X. Luo, *Biosens. Bioelectron.*, 2014, **58**, 153–156.
20 S. Li, Y. Chen, X. He, X. Mao, Y. Zhou, J. Xu and Y. Yang, *Nanoscale Res. Lett.*, 2019, **14**, 1–12.
21 J. Wang, Y. Xu, J. Zhu and P. Ren, *J. Power Sources*, 2012, **208**, 138–143.
22 Y. Xu, H. Bai, G. Lu, C. Li and G. Shi, *J. Am. Chem. Soc.*, 2008, **130**, 5856–5857.
23 X. Peng, L. Meng, W. Zhang, W. Liu, L. Zhang and Y. Zhang, *J. Solid State Electrochem.*, 2015, **20**, 439–447.
24 L. Meng, Y. Xia, W. Liu, L. Zhang, P. Zou and Y. Zhang, *Electrochim. Acta*, 2015, **152**, 330–337.
25 A. Elschner, S. Kirchmeyer, W. Lovenich, U. Merker and K. Reuter, *PEDOT: principles and applications of an intrinsically conductive polymer*, CRC press, 2010.
26 D. Li, M. B. Müller, S. Gilje, R. B. Kaner and G. G. Wallace, *Nat. Nanotechnol.*, 2008, **3**, 101.
27 B. Konkena and S. Vasudevan, *J. Phys. Chem. Lett.*, 2012, **3**, 867–872.
28 Z. Jiang, Y. Shi, Z.-J. Jiang, X. Tian, L. Luo and W. Chen, *J. Mater. Chem. A*, 2014, **2**, 6494–6503.
29 J. M. Yun, J. S. Yeo, J. Kim, H. G. Jeong, D. Y. Kim, Y. J. Noh, S. S. Kim, B. C. Ku and S. I. Na, *Adv. Mater.*, 2011, **23**, 4923–4928.
30 D. Alemu, H.-Y. Wei, K.-C. Ho and C.-W. Chu, *Energy Environ. Sci.*, 2012, **5**, 9662–9671.
31 L. Meng, A. P. Turner and W. C. Mak, *Biosens. Bioelectron.*, 2018, **120**, 115–121.
32 V. H. Pham, T. V. Cuong, S. H. Hur, E. Oh, E. J. Kim, E. W. Shin and J. S. Chung, *J. Mater. Chem.*, 2011, **21**, 3371–3377.
33 M. K. Rabchinskii, V. V. Shnitov, A. T. Dideikin, A. E. Aleksenskii, S. P. Vul', M. V. Baidakova, I. I. Pronin, D. A. Kirilenko, P. N. Brunkov, J. Weise and S. L. Molodtsov, *J. Phys. Chem. C*, 2016, **120**, 28261–28269.
34 G. Greczynski, T. Kugler and W. R. Salaneck, *Thin Solid Films*, 1999, **354**, 129–135.
35 J. T. Han, J. I. Jang, B. H. Jeong, B. J. Kim, S. Y. Jeong, H. J. Jeong, J. H. Cho and G.-W. Lee, *J. Mater. Chem.*, 2012, **22**, 20477–20481.
36 J.-S. Yeo, J.-M. Yun, Y.-S. Jung, D.-Y. Kim, Y.-J. Noh, S.-S. Kim and S.-I. Na, *J. Mater. Chem. A*, 2014, **2**, 292–298.
37 S. Zhang, Y. Shao, H. Liao, M. H. Engelhard, G. Yin and Y. Lin, *ACS Nano*, 2011, **5**, 1785–1791.
38 K. Liu, S. Ronca, E. Andablo-Reyes, G. Forte and S. Rastogi, *Macromolecules*, 2015, **48**, 131–139.
39 H. J. Shin, K. K. Kim, A. Benayad, S. M. Yoon, H. K. Park, I. S. Jung, M. H. Jin, H. K. Jeong, J. M. Kim and J. Y. Choi, *Adv. Funct. Mater.*, 2009, **19**, 1987–1992.
40 H.-L. Guo, P. Su, X. Kang and S.-K. Ning, *J. Mater. Chem. A*, 2013, **1**, 2248–2255.
41 L. Meng, A. P. Turner and W. C. Mak, *ACS Appl. Mater. Interfaces*, 2019, **11**, 34497–34506.
42 B. G. Choi, J. Hong, W. H. Hong, P. T. Hammond and H. Park, *ACS Nano*, 2011, **5**, 7205–7213.
43 N. H. N. Azman, H. N. Lim and Y. Sulaiman, *J. Nanomater.*, 2016, **2016**, 5935402.
44 M. Fan, C. Zhu, L. Liu, Q. Wu, Q. Hao, J. Yang and D. Sun, *Green Chem.*, 2016, **18**, 1731–1737.
45 A. P. Saxena, M. Deepa, A. G. Joshi, S. Bhandari and A. K. Srivastava, *ACS Appl. Mater. Interfaces*, 2011, **3**, 1115–1126.
46 E. Vitoratos, S. Sakkopoulos, E. Dalas, N. Paliatsas, D. Karageorgopoulos, F. Petraki, S. Kennou and S. A. Choulis, *Org. Electron.*, 2009, **10**, 61–66.
47 D. W. Hatchett and M. Josowicz, *Chem. Rev.*, 2008, **108**, 746–769.
48 C. X. Guo, M. Wang, T. Chen, X. W. Lou and C. M. Li, *Adv. Energy Mater.*, 2011, **1**, 736–741.